Determination of the Adsorption Isotherms of Hydrogen and Deuterium Isotopes on a Pt−Ir Alloy in LiOH Solutions Using the Phase-Shift Method and Correlation Constants

Jinyoung Chun,[†] Nam Y. Kim,[‡] and Jang H. Chun*[,‡]

Department of Chemical Engineering, Pohang University of Science and Technology, Pohang, Kyungbuk 790-784, Republic of Korea, and Department of Electronic Engineering, Kwangwoon University, Seoul 139-701, Republic of Korea

The phase-shift method and correlation constants, which are unique electrochemical impedance spectroscopy techniques for studying the linear relationship between the phase shift ($90° \geq -\varphi \geq 0°$) versus electric potential (E) behavior for the optimum intermediate frequency and the fractional surface coverage ($0 \leq \theta \leq 1$) vs E behavior, are proposed and verified to determine the Frumkin, Langmuir, and Temkin adsorption isotherms and related electrode kinetic and thermodynamic parameters. On a Pt−Ir alloy (90:10 mass ratio) in 0.1 M LiOH (H_2O) and 0.1 M LiOH (D_2O) solutions, the Frumkin and Temkin adsorption isotherms (θ vs E), equilibrium constants (K), interaction parameters (g), standard Gibbs energies (ΔG_θ°) of hydrogen (H) and deuterium (D) adsorption, and rates of change (r) of ΔG_θ° of H and D with θ have been determined and are compared using the phase-shift method and correlation constants. The value of K decreases in going from H_2O to D_2O. The values of K for both H and D increase with increasing E and θ. Over the θ range (i.e., $1 \geq \theta \geq 0$), the value of K for H is 3.7 to 4.1 times greater than that for D. For $0.2 < \theta < 0.8$, a lateral attractive ($g < 0$) or repulsive ($g > 0$) interaction between the adsorbed H or D species appears. The duality of the lateral attractive and repulsive interactions is a unique feature of the adsorbed H and D species on Pt, Ir, and Pt−Ir alloys in acidic and alkaline H_2O and D_2O solutions.

Introduction

To obtain an environmentally clean energy source, many experimental methods have been used to study the adsorption of H for the cathodic H_2 evolution reaction (HER) on noble metals (alloys) in acidic and alkaline aqueous solutions. It is well-known that underpotentially deposited hydrogen (UPD H) and overpotentially deposited hydrogen (OPD H) occupy different surface adsorption sites and act as two distinguishable electroadsorbed H species and that only OPD H can contribute to the cathodic HER.[1−6]

Although the Frumkin and Langmuir adsorption isotherms may be regarded as classical models and theories, it is preferable to consider the Frumkin and Langmuir adsorption isotherms for OPD H rather than electrode kinetics and thermodynamics equations for OPD H because these adsorption isotherms are associated more directly with the atomic mechanism of OPD H.[7] However, there is not much reliable information on the Frumkin and Langmuir adsorption isotherms of OPD H and related electrode kinetic and thermodynamic data. Furthermore, there is not much reliable information on the Frumkin and Langmuir adsorption isotherms of overpotentially deposited deuterium (OPD D) for the cathodic D_2 evolution reaction (DER) and related electrode kinetic and thermodynamic data. Hydrogen (OPD H) and deuterium (OPD D) effects have been interesting in electrochemistry, biochemistry, hydrogen technology, nuclear engineering, surface science, and so forth.

* Author to whom correspondence should be addressed. E-mail: jhchun@kw.ac.kr. Fax: +82-2-942-5235. Tel.: +82-2-940-5116.
[†] Pohang University of Science and Technology.
[‡] Kwangwoon University.

Many scientific phenomena have been interpreted by their behavior rather than by their nature. For example, the wave−particle duality of light and electrons (i.e., their wave and particle behaviors) is well-known in science and has been applied in engineering. Notably, these wave and particle behaviors are complementary rather than contradictory to each other. The phase-shift method and correlation constants are unique electrochemical impedance spectroscopy techniques for studying the linear relationship between the phase shift ($90° \geq -\varphi \geq 0°$) versus electric potential (E) behavior for the optimum intermediate frequency and the fractional surface coverage ($0 \leq \theta \leq 1$) vs E behavior of intermediates for sequential reactions on noble and highly corrosion-resistant metals (alloys) in acidic and alkaline H_2O and D_2O solutions.[8−24] The θ versus E behavior of the fractional surface coverage is well-known as the Frumkin or Langmuir adsorption isotherm.[1−7]

New ideas or methods must be rigorously tested, especially when they are unique, but only with pure logic and objectivity and through scientific procedures. However, the objections to the phase-shift method[25−27] do not fulfill these criteria. These objections are substantially attributed to confusion and misunderstanding of the phase-shift method itself.[23,24,28,29] It should especially be noted that all of the objections to the phase-shift method[25,27] can be attributed to confusion and misunderstanding about the applicability of related equations for intermediate frequencies and a unique feature of the Faradaic resistances for the recombination steps.[23,24,30]

To clarify the adsorption isotherms of OPD H and OPD D isotopes, we present and compare the Frumkin and Temkin adsorption isotherms and related electrode kinetic and thermodynamic parameters of a Pt−Ir alloy (90:10 mass ratio) in 0.1 M LiOH (H_2O) and 0.1 M LiOH (D_2O) solutions using the

10.1021/je100418n
Published on Web 11/19/2010

phase-shift method and correlation constants. A negative value of the interaction parameter for the Frumkin adsorption isotherms of OPD H and OPD D isotopes on the Pt−Ir alloy in 0.1 M LiOH (H_2O) and 0.1 M LiOH (D_2O) solutions has also been determined. These aspects have never been discussed elsewhere on the basis of the Frumkin and Temkin adsorption isotherms.

Experimental Section

Preparations. With the H^+ and D^+ concentrations and the effects of the diffuse double layer and pH taken into account,[31] 0.1 M LiOH (H_2O) and 0.1 M LiOH (D_2O) solutions were prepared from LiOH (Alfa Aesar, purity 99.995 %) using purified water (H_2O, resistivity > 18 MΩ·cm) obtained from a Millipore system and heavy water (D_2O, Alfa Aesar, purity 99.8 %), respectively. The pH and pD of the 0.1 M LiOH (H_2O) and 0.1 M LiOH (D_2O) solutions were approximately 12.83 and 13.06, respectively. These solutions were deaerated with 99.999 % purified nitrogen gas for 20 min before the experiments. A standard three-electrode configuration was employed. A saturated calomel electrode (SCE) was used as the standard reference electrode. A platinum−iridium alloy wire (Johnson Matthey, 90:10 Pt/Ir mass ratio, 1.5 mm diameter, estimated surface area ca. 1.06 cm^2) was used as the working electrode. A platinum wire (Johnson Matthey, purity 99.95 %, 1.5 mm diameter, estimated surface area ca. 1.88 cm^2) was used as the counter electrode. Both the Pt−Ir alloy working electrode and the Pt counter electrode were prepared by flame cleaning and then quenched and cooled sequentially in Millipore Milli-Q water and air.

Measurements. A cyclic voltammetry (CV) technique was used to achieve steady states on the Pt−Ir alloy in the 0.1 M LiOH (H_2O) and 0.1 M LiOH (D_2O) solutions. The CV experiments were conducted for 50 cycles at a scan rate of 200 $mV \cdot s^{-1}$ and a scan potential of (−0.241 to 1.0) V versus SCE. The CV technique was also used to confirm the adsorption of OPD H and OPD D isotopes for the cathodic HER and DER on the Pt−Ir alloy in the 0.1 M LiOH (H_2O) and 0.1 M LiOH (D_2O) solutions, respectively. These CV experiments were conducted for 20 cycles at a scan rate of 200 $mV \cdot s^{-1}$ and a scan potential of (0 to −1.0) V versus SCE. After the CV experiments, an electrochemical impedance spectroscopy (EIS) technique was used to study the linear relationship between the $-\varphi$ versus E behavior of the phase shift ($90° \geq -\varphi \geq 0°$) for the optimum intermediate frequency and the θ versus E behavior of the fractional surface coverage ($0 \leq \theta \leq 1$) on the Pt−Ir alloy in the 0.1 M LiOH (H_2O) and 0.1 M LiOH (D_2O) solutions. The EIS experiments were conducted at scan frequencies of (10^4 to 0.1) Hz using a single sine wave, an alternating current (ac) amplitude of 5 mV, and a direct current (dc) potential of (0 to −1.20) V versus SCE.

The CV experiments were performed using an EG&G PAR model 273A potentiostat controlled with the PAR model 270 software package. The EIS experiments were performed using the same apparatus in conjunction with a Schlumberger SI 1255 HF frequency response analyzer controlled with the PAR model 398 software package. To obtain comparable and reproducible results, all of the measurements were carried out using the same preparations, procedures, and conditions at 298 K. As shown in Supplementary Figures 1 and 2 in the Supporting Information, experimental uncertainties in this work were negligible for determining the Frumkin adsorption isotherms. The international sign convention is used: cathodic currents and phase shifts or angles are taken as negative. All potentials are given on the standard hydrogen electrode (SHE) scale. The Gaussian and adsorption isotherm analyses were carried out using the Excel and Origin software packages.

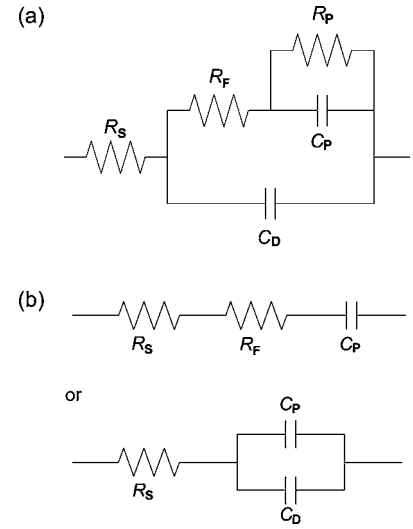

Figure 1. (a) Experimentally proposed equivalent circuit for the phase-shift method. (b) Simplified equivalent circuits for intermediate frequency responses.

Results and Discussion

Theoretical and Experimental Backgrounds of the Phase-Shift Method. The equivalent circuit for the adsorption of OPD H and OPD D for the cathodic HER and DER on the Pt−Ir alloy in the 0.1 M LiOH (H_2O) and 0.1 M LiOH (D_2O) solutions, respectively, can be expressed as shown in Figure 1a.[23,24,32−34] Taking into account the superposition of various effects (relaxation time effects, real surface area problems, surface absorption and diffusion processes, inhomogeneous and lateral interaction effects, oxide layer formation, specific adsorption effects, etc.) that are inevitable under the experimental conditions, we define the equivalent circuit elements as follows: R_S is the real solution resistance; R_F is the real resistance due to the Faradaic resistance for the discharge step (R_ϕ) and superposition of various effects; R_P is the real resistance due to the Faradaic resistance for the recombination step (R_R) and superposition of various effects; C_P is the real capacitance due to the adsorption pseudocapacitance (C_ϕ) and superposition of various effects; and C_D is the real double-layer capacitance. Correspondingly, neither R_F nor C_P is constant; both depend on E and θ and can be measured. It should be noted that both R_ϕ and C_ϕ also depend on E and θ but cannot be measured.

The numerical derivation of C_ϕ from the Frumkin and Langmuir adsorption isotherms (θ vs E) is described elsewhere, and R_ϕ depends on C_ϕ.[32,33] A unique feature of R_ϕ and C_ϕ is that they attain maximum values at $\theta \approx 0.5$ and intermediate E, decrease symmetrically with E at other values of θ, and approach minimum values at $\theta \approx 0$ and low E and at $\theta \approx 1$ and high E; this behavior is well-known in interfacial electrochemistry, electrode kinetics, and EIS.[1−6,32−34] The unique feature and combination of R_ϕ and C_ϕ versus E imply that the normalized rate of change of $-\varphi$ with respect to E, that is, $\Delta(-\varphi)/\Delta E$, corresponds to that of θ versus E, that is, $\Delta\theta/\Delta E$, and vice versa. Both $\Delta(-\varphi)/\Delta E$ and $\Delta\theta/\Delta E$ are maximized at $\theta \approx 0.5$ and intermediate E, decrease symmetrically with E at other values of θ, and are minimized at $\theta \approx 0$ and low E and $\theta \approx 1$ and high E. Notably, this is not a mere coincidence but rather a unique feature of the Frumkin and Langmuir adsorption

isotherms (θ vs E). The linear relationship between and Gaussian profiles of $-\varphi$ versus E or $\Delta(-\varphi)/\Delta E$ and θ versus E or $\Delta\theta/\Delta E$ most clearly appear at the optimum intermediate frequency (f_o). The value of f_o is experimentally and graphically evaluated on the basis of $\Delta(-\varphi)/\Delta E$ and $\Delta\theta/\Delta E$ for intermediate and other frequencies (see Figures 6 to 9). The importance of f_o is described elsewhere.[19] These aspects are the essential nature of the phase-shift method for determining the Frumkin and Langmuir adsorption isotherms.

The frequency responses of the equivalent circuit for all f that is shown in Figure 1a are essential for understanding the unique feature and combination of R_ϕ and C_ϕ versus E, that is, the linear relationship between and Gaussian profiles of $-\varphi$ versus E or $\Delta(-\varphi)/\Delta E$ and θ versus E or $\Delta\theta/\Delta E$ at f_o. At very low frequencies, the equivalent circuit for all f can be expressed as a series circuit of R_S, R_F, and R_P. At very high frequencies, the equivalent circuit for all f can be expressed as a series circuit of R_S and C_D. At intermediate frequencies, one finds regions in which the equivalent circuit for all f behaves as a series circuit of R_S, R_F, and C_P or a series and parallel circuit of R_S, C_P, and C_D, as shown in Figure 1b.[23,24,32,33] However, it should be noted that the simplified equivalent circuit shown in Figure 1b does not represent the change of the cathodic HER and DER themselves but only the intermediate-frequency response.

At intermediate frequencies, the impedance (Z) and phase shift ($-\varphi$) are given by[23,24]

$$Z = R_S + R_F - \frac{j}{\omega C_P} \tag{1a}$$

$$-\varphi = \arctan\left[\frac{1}{\omega(R_S + R_F)C_P}\right] \tag{1b}$$

for the upper circuit in Figure 1b or

$$Z = R_S - \frac{j}{\omega(C_P + C_D)} \tag{2a}$$

$$-\varphi = \arctan\left[\frac{1}{\omega R_S(C_P + C_D)}\right] \tag{2b}$$

for the lower circuit in Figure 1b, where j is the imaginary unit (i.e., $j^2 = -1$) and ω is the angular frequency, defined as $\omega = 2\pi f$, where f is the frequency. Under these conditions,

$$R_P \gg \frac{1}{\omega C_P} \quad \text{and} \quad R_P \gg R_S + R_F \tag{3}$$

In our previously published papers, only eq 1a was used with a footnote stating that C_P practically includes C_D (see Tables 1 and 2 in ref 18, Table 1 in ref 17, etc.). Both eqs 1a and 2a show that the effect of R_P on $-\varphi$ for intermediate frequencies is negligible. These aspects are completely overlooked, confused, and misunderstood in the comments on the phase-shift method by Horvat-Radošević, Kvastek, and Lasia.[25−27] Correspondingly, all of the simulations of the phase-shift method using eq 1a that appear in these comments (where C_P does not include C_D)[25−27] are basically invalid or wrong. All of the analyses of the effect of R_P on $-\varphi$ for intermediate frequencies are also invalid or wrong (see the Supporting Information).[23,24,30]

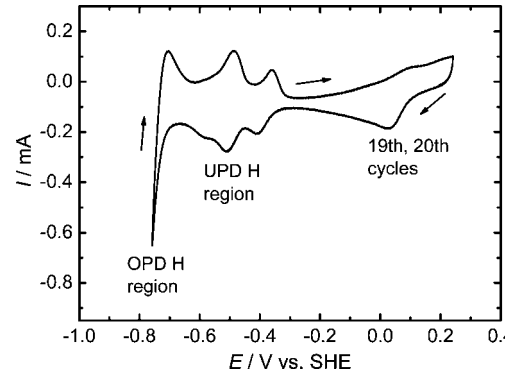

Figure 2. Cyclic voltammogram for the cathodic HER on the Pt−Ir alloy in 0.1 M LiOH (H_2O) solution. Number of cycles, 20; stored cycles, 19th and 20th; scan rate, 200 mV·s^{-1}; scan potential range, (0.241 to −0.759) V vs SHE.

The following limitations and conditions of the equivalent circuit elements for f_o are summarized on the basis of the experimental data.[23,24] Neither R_S nor C_D is constant. At $\theta \approx 0$, $R_S > R_F$ and $C_D > C_P$, or vice versa, and so forth. For a wide range of θ ($0.2 < \theta < 0.8$), $R_F \gg R_S$ or $R_F > R_S$ and $C_P \gg C_D$ or $C_P > C_D$, and so forth. At $\theta \approx 1$, $R_S > R_F$ or $R_S < R_F$ and $C_P \gg C_D$. The measured $-\varphi$ for f_o depends on E and θ. In contrast to numerical calculations or analyses, these limitations and conditions for eq 1a or 2a are not considered for the phase-shift method because all of the measured values of $-\varphi$ for intermediate frequencies include (R_S, R_F) and (C_P, C_D). Correspondingly, the measured $-\varphi$ for f_o is valid and correct regardless of the applicability of eq 1a or 2a and related limitations and conditions (see Supplementary Tables 3 and 4 in the Supporting Information). This is the reason why the phase-shift method is the most useful and effective way to determine adsorption isotherms.

The unique feature and combination of (R_S, R_F) and (C_P, C_D) are equivalent to those of R_ϕ and C_ϕ. This is attributed to the reciprocal property of R_F and C_P and suggests that only the polar form of the equivalent circuit impedance, that is, $-\varphi$ described in eq 1b or 2b, is useful and effective for studying the linear relationship between the $-\varphi$ vs E behavior ($90° \geq -\varphi \geq 0°$) at f_o and the θ vs E behavior ($0 \leq \theta \leq 1$). It should be noted that the phase-shift method for determining adsorption isotherms has been proposed and verified on the basis of the phase-shift curves ($-\varphi$ vs log f) at various E (see Figures 4 and 5). These aspects have been experimentally and consistently verified and discussed in our previously published papers.[8−24] As stated above, the unique feature and combination of R_ϕ and C_ϕ versus E, that is, $-\varphi$ versus E or $\Delta(-\varphi)/\Delta E$ and θ versus E or $\Delta\theta/\Delta E$, most clearly appear at f_o. The linear relationship between and Gaussian profiles of $-\varphi$ versus E or $\Delta(-\varphi)/\Delta E$ and θ versus E or $\Delta\theta/\Delta E$ for f_o imply that only one Frumkin or Langmuir adsorption isotherm is determined on the basis of the relevant experimental results (see Figures 6 to 9). The shape and location of the $-\varphi$ versus E or $\Delta(-\varphi)/\Delta E$ curve and the θ versus E or $\Delta\theta/\Delta E$ curve for f_o correspond to the interaction parameter (g) and equilibrium constant (K_o) for the Frumkin or Langmuir adsorption isotherm, respectively. This is another reason why the phase-shift method is the most accurate way to determine adsorption isotherms.

Basic Procedure and Description of the Phase-Shift Method. Figures 2 and 3 show the cyclic voltammograms for the cathodic HER and DER on the Pt−Ir alloy in the 0.1 M LiOH (H_2O) and 0.1 M LiOH (D_2O) solutions, respectively. Figures 2 and 3 also show that the 19th and 20th cyclic

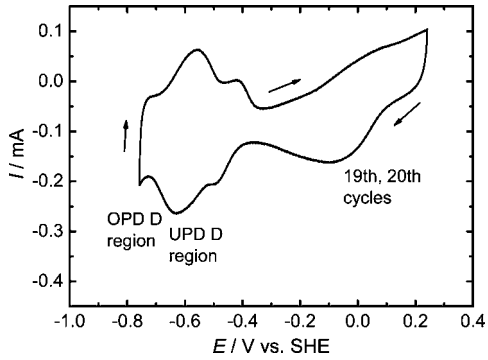

Figure 3. Cyclic voltammogram for the cathodic DER on the Pt−Ir alloy in 0.1 M LiOH (D_2O) solution. Number of cycles, 20; stored cycles, 19th and 20th; scan rate, 200 mV·s^{-1}; scan potential range, (0.241 to −0.759) V vs SHE.

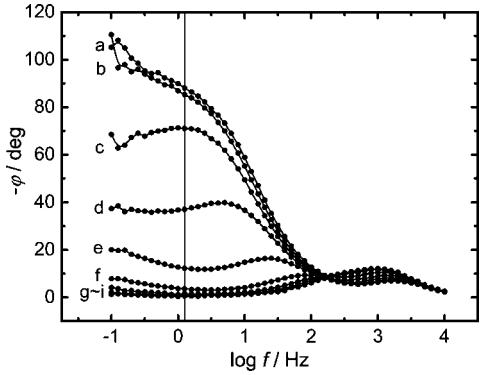

Figure 4. Comparison of the phase-shift curves ($-\varphi$ vs log f) for different potentials (E) on the Pt−Ir alloy in 0.1 M LiOH (H_2O) solution. Measured values: ●. Vertical solid line, 1.259 Hz; single sine wave; scan frequency range, (10^4 to 0.1) Hz; ac amplitude, 5 mV. Dc potentials: (a) −0.659 V; (b) −0.684 V; (c) −0.709 V; (d) −0.734 V; (e) −0.759 V; (f) −0.784 V; (g) −0.809 V; (h) −0.834 V; (i) −0.859 V (all vs SHE).

voltammograms completely overlap. One can interpret this to mean that steady states have been achieved. In contrast to acidic aqueous solutions,[2−6,9] Figure 2 suggests that the adsorption of UPD H and OPD H is distinguishable using the phase-shift method for determining adsorption isotherms (see Figure 10 in ref 9). Notably, the transition between the adsorption isotherms of UPD H and OPD H shown in ref 9 is associated with the atomic mechanisms of UPD H and OPD H, that is, the adsorption sites of UPD H and OPD H.[7] Similarly, Figure 3 suggests that the adsorption of UPD D and OPD D is distinguishable using the phase-shift method for determining adsorption isotherms.

In Figure 2, the UPD H hydrogen adsorption peaks due to hydrogen reduction occur sequentially at approximately (−0.417 and −0.511) V versus SHE. The UPD H hydrogen desorption peaks due to hydrogen oxidation occur sequentially at approximately (−0.489 and −0.359) V versus SHE. The adsorption of OPD H occurs at approximately −0.659 V versus SHE. In Figure 3, the UPD D deuterium adsorption peaks due to deuterium reduction occur sequentially at approximately (−0.509 and −0.629) V versus SHE. The UPD D deuterium desorption peaks due to deuterium oxidation occur sequentially at approximately (−0.561 and −0.421) V versus SHE. The adsorption of OPD D occurs at approximately −0.709 V versus SHE. In the following discussions, H and D mean OPD H and OPD D, respectively.

Figures 4 and 5 compare the phase-shift curves ($-\varphi$ vs log f) for different potentials (E) on the Pt−Ir alloy in the 0.1 M LiOH (H_2O) and 0.1 M LiOH (D_2O) solutions, respectively.

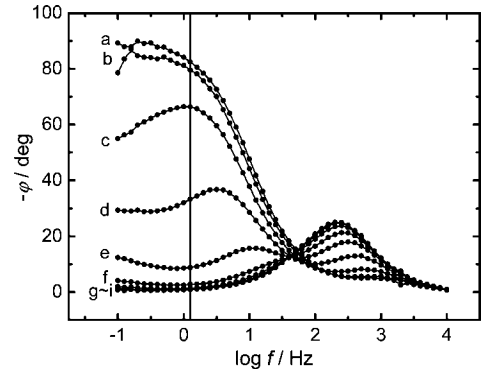

Figure 5. Comparison of the phase-shift curves ($-\varphi$ vs log f) for different potentials (E) on the Pt−Ir alloy in 0.1 M LiOH (D_2O) solution. Measured values: ●. Vertical solid line, 1.259 Hz; single sine wave; scan frequency range, (10^4 to 0.1) Hz; ac amplitude, 5 mV. Dc potentials: (a) −0.709 V; (b) −0.734 V; (c) −0.759 V; (d) −0.784 V; (e) −0.809 V; (f) −0.834 V; (g) −0.859 V; (h) −0.884 V; (i) −0.909 V (all vs SHE).

Table 1. Measured Values of the Phase Shift ($-\varphi$), the Estimated Fractional Surface Coverage (θ) of H, and the Normalized Change Rate [$\Delta(-\varphi)/\Delta E = \Delta\theta/\Delta E$] on the Pt−Ir Alloy in 0.1 M LiOH (H_2O) Solution at the Optimum Intermediate Frequency (f_o = 1.259 Hz)

E/V vs SHE	$-\varphi$/deg	θ	change rate
−0.659	88.0	∼0	∼0
−0.684	85.3	0.03089	0.24714
−0.709	71.0	0.19451	1.30892
−0.734	37.1	0.58238	3.10297
−0.759	12.3	0.86613	2.27002
−0.784	3.6	0.96568	0.79634
−0.809	1.6	0.98856	0.18307
−0.834	0.9	0.99657	0.06407
−0.859	0.6	∼1	0.02746

The intermediate frequency of 1.259 Hz, shown as a vertical solid line on the $-\varphi$ versus log f plots in Figures 4 and 5, can be set as f_o for $-\varphi$ versus E and θ versus E. At the maximum $-\varphi$ shown in curves a of Figures 4 and 5, it appears that the adsorption of H and D and superposition of various effects are minimized; that is, $\theta \approx 0$ and E is low. It should be noted that θ ($0 \le \theta \le 1$) depends on E. At the maximum $-\varphi$, when $\theta \approx 0$ and E is low, both $\Delta(-\varphi)/\Delta E$ and $\Delta\theta/\Delta E$ are minimized because R_ϕ and C_ϕ approach minimum values. At the minimum $-\varphi$, shown in curves i of Figures 4 and 5, it appears that the adsorption of H and D and superposition of various effects are maximized or almost saturated; that is, $\theta \approx 1$ and E is high. At the minimum $-\varphi$, when $\theta \approx 1$ and E is high, both $\Delta(-\varphi)/\Delta E$ and $\Delta\theta/\Delta E$ are also minimized because R_ϕ and C_ϕ approach minimum values. At the medium $-\varphi$ between curves c and d in Figures 4 and 5, it appears that both $\Delta(-\varphi)/\Delta E$ and $\Delta\theta/\Delta E$ are maximized because R_ϕ and C_ϕ approach maximum values at $\theta \approx 0.5$ and intermediate E (see Tables 1 and 2 and Figures 8b and 9b).

The procedure and description of the phase-shift method for determining the Frumkin adsorption isotherms of H and D on the Pt−Ir alloy in the 0.1 M LiOH (H_2O) and 0.1 M LiOH (D_2O) solutions are briefly summarized in Tables 1 and 2, respectively. Tables 1 and 2 show the values of $-\varphi$ and θ as functions of E at f_o = 1.259 Hz with −25 mV increment changes in E on the Pt−Ir alloy in the 0.1 M LiOH (H_2O) and 0.1 M LiOH (D_2O) solutions, respectively. The values of $-\varphi$ and θ as functions of E at f_o = 1.259 Hz shown in Figures 6 and 7 are illustrated on the basis of the experimental results summarized in Tables 1 and 2, respectively. The values of $-\varphi$ and θ as functions of E at other frequencies (0.1 Hz, 10 Hz, and

Table 2. Measured Values of the Phase Shift ($-\varphi$), the Estimated Fractional Surface Coverage (θ) of D, and the Normalized Change Rate [$\Delta(-\varphi)/\Delta E = \Delta\theta/\Delta E$] on the Pt−Ir Alloy in 0.1 M LiOH (D_2O) Solution at the Optimum Intermediate Frequency ($f_o = 1.259$ Hz)

E/V vs SHE	$-\varphi$/deg	θ	change rate
−0.709	82.4	~0	~0
−0.734	79.6	0.03431	0.27451
−0.759	66.4	0.19608	1.29412
−0.784	33.3	0.60172	3.24510
−0.809	8.8	0.90196	2.40196
−0.834	2.7	0.97672	0.59804
−0.859	1.3	0.99387	0.13725
−0.884	1.1	0.99632	0.01961
−0.909	0.8	~1	0.02941

100 Hz) shown in Figures 6 and 7 are also illustrated through the same procedures summarized in Tables 1 and 2, respectively.

As shown in Figures 4 and 5, $-\varphi$ depends on both f and E. However, θ depends on only E. As previously described, the linear relationship between and Gaussian profiles of $-\varphi$ versus E or $\Delta(-\varphi)/\Delta E$ and θ versus E or $\Delta\theta/\Delta E$ most clearly appear at f_o. This is the reason why the comparison of $-\varphi$ versus E and θ versus E for different frequencies shown in Figures 6 and 7 is necessary to determine f_o. It should be noted that the $-\varphi$ versus E profiles shown in Figures 6a and 7a correspond to the θ versus E profiles shown in Figures 6b and 7b and vice versa. The differences between the $-\varphi$ versus E and θ versus E profiles at $f_o = 1.259$ Hz and those at other frequencies (0.1 Hz, 10 Hz, 100 Hz) shown in Figures 6 and 7 do not represent the measurement error but only the frequency response.

Figures 8 and 9 compare the normalized rates of change of $-\varphi$ and θ with respect to E, that is, $\Delta(-\varphi)/\Delta E$ and $\Delta\theta/\Delta E$, for four different frequencies (0.1 Hz, 1.259 Hz, 10 Hz, and 100 Hz) on the Pt−Ir alloy in the 0.1 M LiOH (H_2O) and 0.1

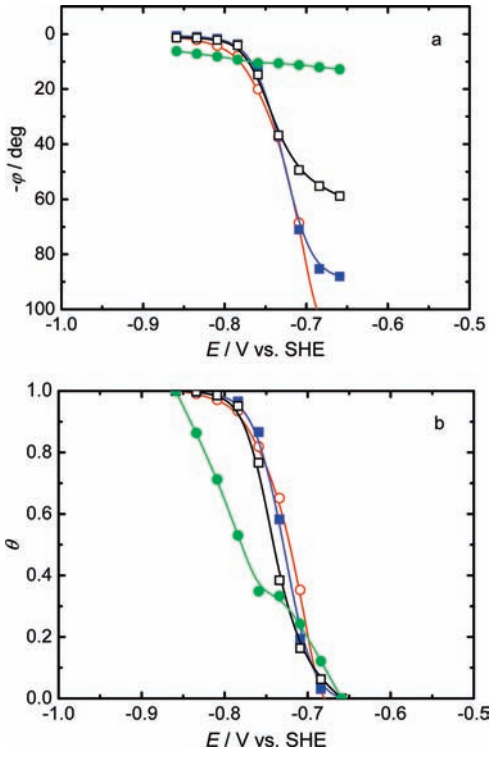

Figure 6. Comparison of (a) the phase-shift profiles ($-\varphi$ vs E) and (b) the surface-coverage profiles (θ vs E) at four different frequencies on the Pt−Ir alloy in 0.1 M LiOH (H_2O) solution. Measured or estimated values: ○, 0.1 Hz; ■, 1.259 Hz; □, 10 Hz; ●, 100 Hz. The optimum intermediate frequency (f_o) is 1.259 Hz.

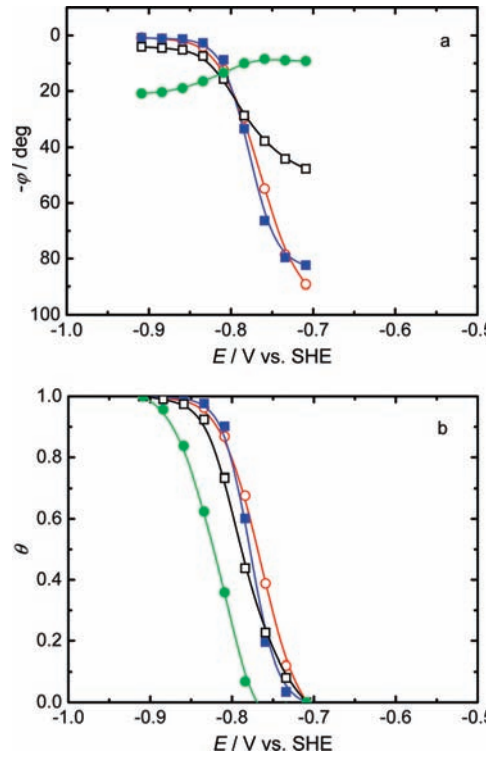

Figure 7. Comparison of (a) the phase-shift profiles ($-\varphi$ vs E) and (b) the surface-coverage profiles (θ vs E) at four different frequencies on the Pt−Ir alloy in 0.1 M LiOH (D_2O) solution. Measured or estimated values: ○, 0.1 Hz; ■, 1.259 Hz; □, 10 Hz; ●, 100 Hz. The optimum intermediate frequency (f_o) is 1.259 Hz.

M LiOH (D_2O) solutions, respectively. The Gaussian profiles shown in Figures 8b and 9b are based on the $\Delta(-\varphi)/\Delta E$ and $\Delta\theta/\Delta E$ data for $f_o = 1.259$ Hz summarized in Tables 1 and 2, respectively. Similarly, the Gaussian profiles for other frequencies (0.1 Hz, 10 Hz, and 100 Hz) shown in Figures 8 and 9 were obtained through the same procedures summarized in Tables 1 and 2, respectively. In Figures 8b and 9b, $\Delta(-\varphi)/\Delta E$ corresponds to $\Delta\theta/\Delta E$ and vice versa. Both $\Delta(-\varphi)/\Delta E$ and $\Delta\theta/\Delta E$ are maximized at the medium $-\varphi$ when $\theta \approx 0.5$ and E is intermediate, decrease symmetrically with E at other values of θ, and are minimized at the maximum $-\varphi$ when $\theta \approx 0$ and E is low and the minimum $-\varphi$ when $\theta \approx 1$ and E is high. As previously described, this is a unique feature of the Frumkin and Langmuir adsorption isotherms. The shape and location of the $-\varphi$ versus E or $\Delta(-\varphi)/\Delta E$ curve and the θ versus E or $\Delta\theta/\Delta E$ curve at f_o correspond to the interaction parameter (g) and equilibrium constant (K_o) for the Frumkin or Langmuir adsorption isotherm, respectively. Figures 8a and 9a show that the low-frequency response, that is, the effect of R_P on $-\varphi$, appears at 0.1 Hz. Figures 8d and 9d show that the high-frequency response, that is, the effect of R_S and C_D on $-\varphi$, appears at 100 Hz. The differences between the Gaussian profiles of $\Delta(-\varphi)/\Delta E$ and $\Delta\theta/\Delta E$ at $f_o = 1.259$ Hz and those at other frequencies (0.1 Hz, 10 Hz, and 100 Hz) shown in Figures 8 and 9 do not represent the measurement error but only the frequency response.

Finally, one can conclude that the Frumkin or Langmuir adsorption isotherm corresponding to $\Delta(-\varphi)/\Delta E$ and $\Delta\theta/\Delta E$ at f_o is readily determined. The linear relationship between and Gaussian profiles of the $-\varphi$ versus E or $\Delta(-\varphi)/\Delta E$ curve and the θ versus E or $\Delta\theta/\Delta E$ curve at f_o express the essential nature of the phase-shift method for determining the Frumkin or Langmuir adsorption isotherm. Notably, this is not valid and correct at all f and E but only at f_o for a limited range of E.

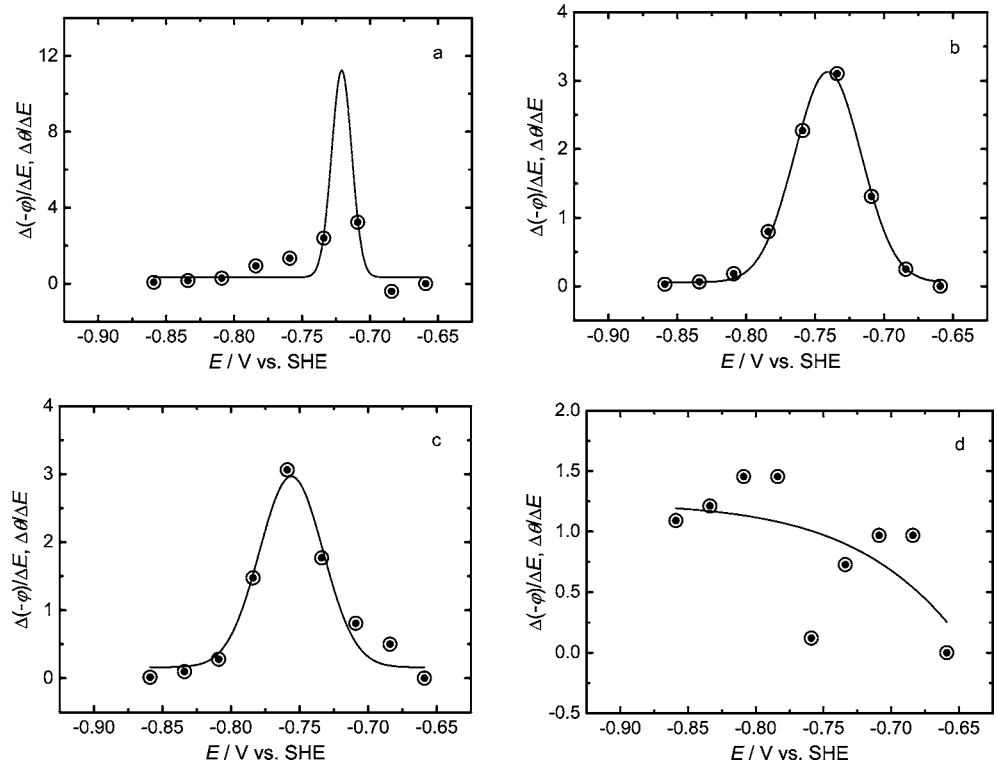

Figure 8. Comparison of the normalized rates of change of $-\varphi$ and θ with respect to E, that is, $\Delta(-\varphi)/\Delta E$ and $\Delta\theta/\Delta E$, at four different frequencies on the Pt−Ir alloy in 0.1 M LiOH (H_2O) solution: —, fitted Gaussian profile; ○, $\Delta(-\varphi)/\Delta E$; ●, $\Delta\theta/\Delta E$. Frequencies: (a) 0.1 Hz; (b) 1.259 Hz; (c) 10 Hz; (d) 100 Hz. The optimum intermediate frequency (f_o) is 1.259 Hz.

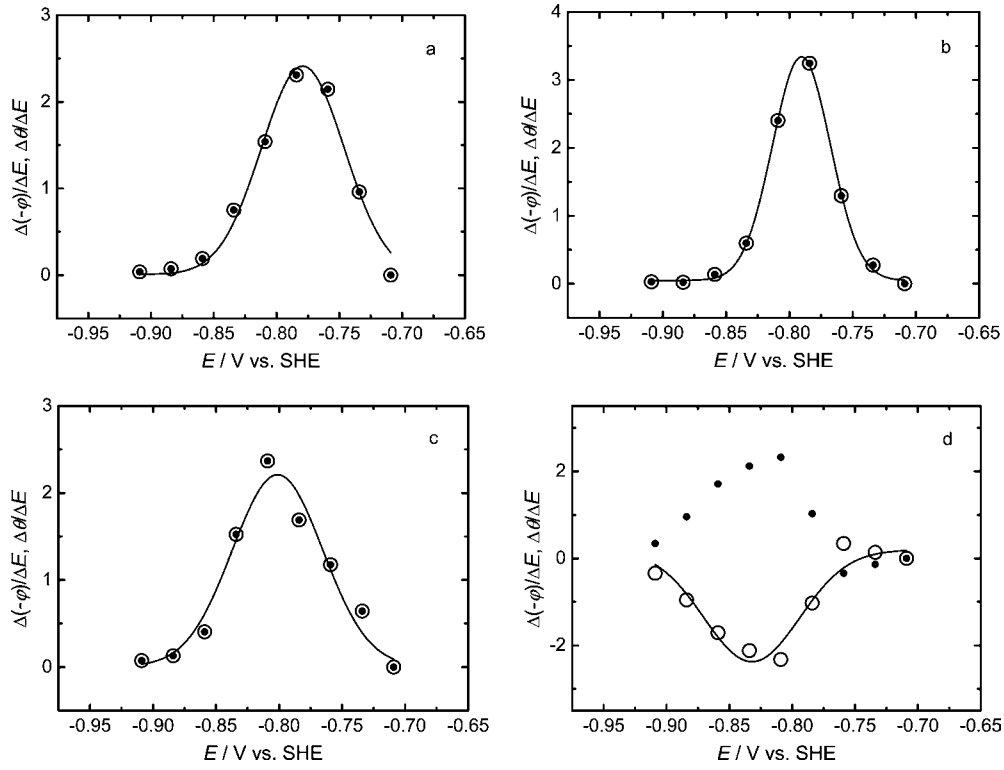

Figure 9. Comparison of the normalized rates of change of $-\varphi$ and θ with respect to E, that is, $\Delta(-\varphi)/\Delta E$ and $\Delta\theta/\Delta E$, at four different frequencies on the Pt−Ir alloy in 0.1 M LiOH (D_2O) solution: —, fitted Gaussian profile; ○, $\Delta(-\varphi)/\Delta E$; ●, $\Delta\theta/\Delta E$. Frequencies: (a) 0.1 Hz; (b) 1.259 Hz; (c) 10 Hz; (d) 100 Hz. The optimum intermediate frequency (f_o) is 1.259 Hz.

Frumkin, Langmuir, and Temkin Adsorption Isotherms. The derivation and interpretation of the practical forms of the electrochemical Frumkin, Langmuir, and Temkin adsorption isotherms are described elsewhere.[35−37] The Frumkin adsorption isotherm assumes that the Pt−Ir alloy surface is inhomogeneous or that the lateral interaction effect is not negligible. The Frumkin adsorption isotherm can be expressed as follows:[36]

$$\frac{\theta}{1-\theta}\exp(g\theta) = K_o C^+ \exp(-EF/RT) \quad (4)$$

$$g = \frac{r}{RT} \quad (5)$$

$$K = K_o \exp(-g\theta) \quad (6)$$

where θ ($0 \le \theta \le 1$) is the fractional surface coverage, g is the interaction parameter for the Frumkin adsorption isotherm, K_o is the equilibrium constant at $g = 0$, C^+ is the concentration of ions (H^+, D^+) in the bulk solution, E is the negative potential, F is Faraday's constant, R is the gas constant, T is the absolute temperature, r is the rate of change of the standard Gibbs energy of adsorption with θ, and K is the equilibrium constant. The dimension of K is described elsewhere.[38] It should be noted that when $g = 0$ in eqs 4 to 6, the Langmuir adsorption isotherm is obtained. For the Langmuir adsorption isotherm, when $g = 0$, the inhomogeneous and lateral interaction effects on the adsorption are assumed to be negligible.

On the Pt−Ir alloy in the 0.1 M LiOH (H_2O) and 0.1 M LiOH (D_2O) solutions, the numerically calculated Frumkin adsorption isotherms of H and D using eq 4 are shown in Figures 10 and 11, respectively. Curves a, b, and c in Figure 10 show the three numerically calculated Frumkin adsorption isotherms of H corresponding to $g = 0$, -2.2, and -5.5, respectively, for $K_o = 8.6 \cdot 10^{-5}$ mol^{-1}. Curve a, with $g = 0$ for $K_o = 8.6 \cdot 10^{-5}$ mol^{-1}, corresponds to the Langmuir adsorption isotherm, that is, $K = 8.6 \cdot 10^{-5}$ mol^{-1}. Curve b shows that the Frumkin adsorption isotherm $K = 8.6 \cdot 10^{-5} \exp(2.2\theta)$ mol^{-1} is applicable to the adsorption of H, and eq 5 gives $r = -5.5$ kJ·mol^{-1}. On the other hand, curves a, b, and c of Figure 11 show the three numerically calculated Frumkin adsorption isotherms of D corresponding to $g = 0$, -2.3, and -5.5, respectively, for $K_o = 2.1 \cdot 10^{-5}$ mol^{-1}. As in Figure 10, curve a in Figure 11, with $g = 0$ for $K_o = 2.1 \cdot 10^{-5}$ mol^{-1}, corresponds to the Langmuir adsorption isotherm, that is, $K = 2.1 \cdot 10^{-5}$ mol^{-1}. Curve b shows that the Frumkin adsorption isotherm $K = 2.1 \cdot 10^{-5} \exp(2.3\theta)$ mol^{-1} is applicable to the adsorption of D, and eq 5 gives $r = -5.7$ kJ·mol^{-1}. The numerical comparison of the K values for the Frumkin adsorption isotherms of H and D over the θ range $0 \le \theta \le 1$ is summarized in Table 3. The value of K decreases in going from H_2O to D_2O. The values of K for both H and D increase with increasing E and θ. Over the θ range (i.e., $1 \ge \theta \ge 0$), the value of K for H is 3.7 to 4.1 times greater than that for D.

At intermediate values of θ (i.e., $0.2 < \theta < 0.8$), the pre-exponential term, $\theta/(1-\theta)$, varies little with θ in comparison with the variation of the exponential term, $\exp(g\theta)$ (see eq 4). Under these approximate conditions, the Temkin adsorption isotherm can be simply derived from the Frumkin adsorption isotherm. The Temkin adsorption isotherm can be expressed as follows:[36]

$$\exp(g\theta) = K_o C^+ \exp(-EF/RT) \quad (7)$$

Figures 12 and 13 show the determination of the Temkin adsorption isotherms corresponding to the Frumkin adsorption isotherms shown in curves b of Figures 10 and 11, respectively. The dashed line labeled b in Figure 12 shows that the numerically calculated Temkin adsorption isotherm of H using eq 7 is $K = 8.6 \cdot 10^{-4} \exp(-2.4\theta)$ mol^{-1}, and eq 5 gives $r = 6.0$ kJ·mol^{-1}. On the other hand, the dashed line labeled b in Figure 13 shows that the numerically calculated Temkin adsorption isotherm of D using eq 7 is $K = 2.1 \cdot 10^{-4} \exp(-2.3\theta)$ mol^{-1}, for which eq 5 gives $r = 5.7$ kJ·mol^{-1}. The numerical comparison of the K values for the Temkin adsorption isotherms of H and D over the θ range $0.2 < \theta < 0.8$ is summarized in Table 4. It should be noted that the Temkin adsorption isotherms of H and D represented by the dashed lines b in Figures 12 and 13 are valid and effective only for $0.2 < \theta < 0.8$. For $0.8 > \theta > 0.2$, the value of K for H is approximately 3.9 to 4.1 times greater than that for D.

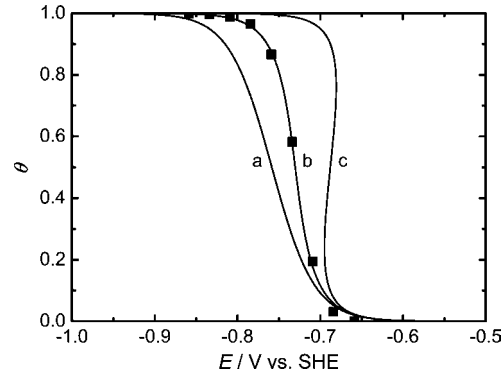

Figure 10. Comparison of the experimental and fitted data for the Frumkin adsorption isotherms (θ vs E) of H on the Pt−Ir alloy in 0.1 M LiOH (H_2O) solution. Experimental data: ■. Solid curves show values calculated using eq 4 (the Frumkin adsorption isotherm) for (a) $g = 0$, (b) $g = -2.2$, and (c) $g = -5.5$ with $K_o = 8.6 \cdot 10^{-5}$ mol^{-1}. The Frumkin adsorption isotherm shown in curve b of Figure 10 is $K = 8.6 \cdot 10^{-5} \exp(2.2\theta)$ mol^{-1}.

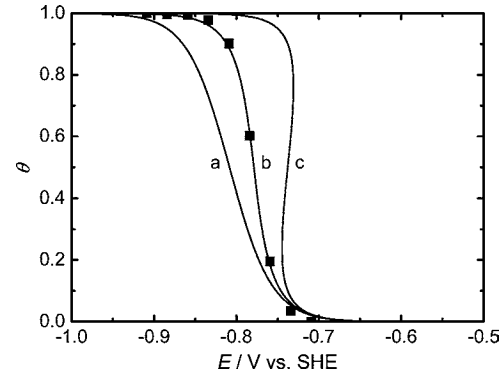

Figure 11. Comparison of the experimental and fitted data for the Frumkin adsorption isotherms (θ vs E) of D on the Pt−Ir alloy in 0.1 M LiOH (D_2O) solution. Experimental data: ■. Solid curves show values calculated using eq 4 (the Frumkin adsorption isotherm) for (a) $g = 0$, (b) $g = -2.3$, and (c) $g = -5.5$ with $K_o = 2.1 \cdot 10^{-5}$ mol^{-1}. The Frumkin adsorption isotherm shown in curve b of Figure 11 is $K = 2.1 \cdot 10^{-5} \exp(2.3\theta)$ mol^{-1}.

The applicability of the Frumkin and Temkin adsorption isotherms over the same potential range is described elsewhere.[23] As shown in dashed lines b in Figures 12 and 13, the Temkin adsorption isotherms are valid and effective only for $0.2 < \theta < 0.8$. This θ range corresponds to a short potential range (ca. 37 mV). For other values of θ, that is, $0 \le \theta < 0.2$ and $0.8 < \theta \le 1$, only the Frumkin adsorption isotherms are applicable. Consequently, one can conclude that the Frumkin adsorption isotherm is more accurate, useful, and effective than the Temkin adsorption isotherm.

Correlation Constants between the Adsorption Isotherms. As previously described, the Frumkin, Langmuir, and Temkin adsorption conditions are different from each other. Only one Frumkin or Langmuir adsorption isotherm is determined on the

Table 3. Comparison of the Standard Gibbs Energies of Adsorption (ΔG_θ°) of H and D, the Equilibrium Constants (K) for the Frumkin Adsorption Isotherms, and the Rates of Change (r) of the Standard Gibbs Energies of Adsorption of H and D with Fractional Surface Coverage (θ) on the Pt−Ir Alloy in the 0.1 M LiOH (H_2O) and 0.1 M LiOH (D_2O) Solutions[a]

		ΔG_θ°	K	r
solution	adsorbate	kJ·mol^{-1}	mol^{-1}	kJ·mol^{-1}
0.1 M LiOH (H_2O)	H	$23.2 \geq \Delta G_\theta^\circ \geq 17.7$	$8.6\cdot10^{-5} \leq K^b \leq 7.8\cdot10^{-4}$	−5.5
0.1 M LiOH (D_2O)	D	$26.7 \geq \Delta G_\theta^\circ \geq 21.0$	$2.1\cdot10^{-5} \leq K^c \leq 2.1\cdot10^{-4}$	−5.7

[a] The Frumkin adsorption isotherms are valid and effective for $0 \leq \theta \leq 1$. [b] $K = 8.6\cdot10^{-5} \exp(2.2\theta)$ mol^{-1}. [c] $K = 2.1\cdot10^{-5} \exp(2.3\theta)$ mol^{-1}.

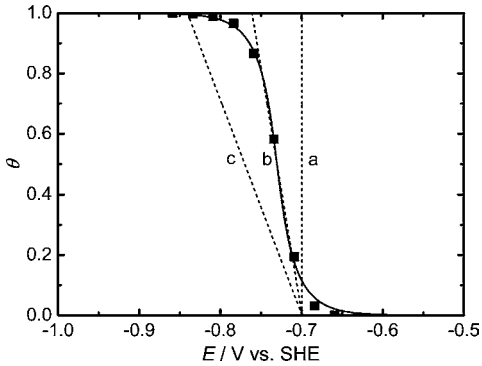

Figure 12. Comparison of the experimentally determined Frumkin adsorption isotherm and three fitted Temkin adsorption isotherms (θ vs E) of H on the Pt−Ir alloy in 0.1 M LiOH (H_2O) solution. Experimental data: ■. The solid curve shows the Frumkin adsorption isotherm calculated using eq 4. Dashed lines show values calculated using eq 7 (the Temkin adsorption isotherm) and the correlation constants for (a) $g = 0$, (b) $g = 2.4$, and (c) $g = 5.5$ with $K_o = 8.6\cdot10^{-4}$ mol^{-1}. The Temkin adsorption isotherm shown in dashed line b in Figure 12, $K = 8.6\cdot10^{-4} \exp(-2.4\theta)$ mol^{-1}, is valid and effective only for $0.2 < \theta < 0.8$.

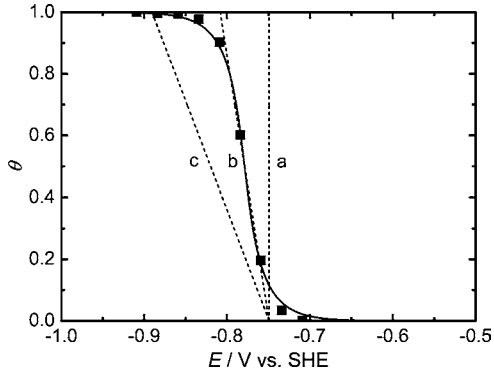

Figure 13. Comparison of the experimentally determined Frumkin adsorption isotherm and three fitted Temkin adsorption isotherms (θ vs E) of D on the Pt−Ir alloy in 0.1 M LiOH (D_2O) solution. Experimental data: ■. The solid curve shows the Frumkin adsorption isotherm calculated using eq 4. Dashed lines show values calculated using eq 7 (the Temkin adsorption isotherm) and the correlation constants for (a) $g = 0$, (b) $g = 2.3$, and (c) $g = 5.5$ with $K_o = 2.1\cdot10^{-4}$ mol^{-1}. The Temkin adsorption isotherm shown in dashed line b in Figure 13, $K = 2.1\cdot10^{-4} \exp(-2.3\theta)$ mol^{-1}, is valid and effective only for $0.2 < \theta < 0.8$.

basis of the relevant experimental results (see Figures 6 to 11). However, the two different adsorption isotherms, that is, the Temkin and Frumkin or Langmuir adsorption isotherms, appear to fit the same data for $0.2 < \theta < 0.8$. This unique feature of the Temkin and Frumkin or Langmuir adsorption isotherms has been experimentally and consistently verified using the phase-shift method and correlation constants.[17−24] For $0.2 < \theta < 0.8$, the Temkin adsorption isotherm correlating with the Frumkin or Langmuir adsorption isotherm, and vice versa, is readily determined using the correlation constants (see Figures 12 and 13).

In this work, one can also confirm that the values of g and K_o for the Temkin adsorption isotherm are approximately 4.6 and 10 times greater than those for the correlated Frumkin or Langmuir adsorption isotherm, respectively. These factors (ca. 4.6 and 10) can be taken as correlation constants between the Temkin and Frumkin or Langmuir adsorption isotherms. The two different adsorption isotherms, that is, the Temkin and Frumkin or Langmuir adsorption isotherms, appear to fit the same data regardless of their adsorption conditions. This aspect is described elsewhere.[17,18,21]

Negative Value of the Interaction Parameter. A negative value of the interaction parameter (g) for the Frumkin adsorption isotherm is qualitatively and quantitatively interpreted elsewhere.[36,39] The negative values of g for the Frumkin adsorption isotherms shown in curves b in Figures 10 and 11 imply a lateral attractive interaction between the adsorbed H or D species, which leads to an increase in the absolute value of the standard Gibbs energies of adsorption ($|\Delta G_\theta^\circ|$) of H and D with θ ($0 \leq \theta \leq 1$) (see Table 3). This interaction is a unique feature of the Frumkin adsorption isotherms of H and D on Pt, Ir, and Pt−Ir alloys in acidic and alkaline H_2O and D_2O solutions.[20] On the other hand, the positive values of g for the Temkin adsorption isotherms shown in dashed lines b in Figures 12 and 13 imply a lateral repulsive interaction between the adsorbed H or D species, which leads to a decrease in $|\Delta G_\theta^\circ|$ of H and D with θ ($0.2 < \theta < 0.8$) (see Table 4). As shown in straight lines b in Figures 12 and 13, the region $0.2 < \theta < 0.8$ corresponds to the short potential range (ca. 37 mV), which is difficult to observe in the Temkin adsorption isotherms correlating with the Frumkin adsorption isotherms. It is understood that the observation of the lateral repulsive interaction between the adsorbed H or D species is difficult using other conventional methods. Consequently, one can conclude that the lateral attractive ($g < 0$) or repulsive ($g > 0$) interaction between the adsorbed H or D species appears at $0.2 < \theta < 0.8$. The duality of the lateral

Table 4. Comparison of the Standard Gibbs Energies of Adsorption (ΔG_θ°) of H and D, the Equilibrium Constants (K) for the Temkin Adsorption Isotherms, and the Rates of Change (r) of the Standard Gibbs Energies of Adsorption of H and D with Fractional Surface Coverage (θ) on the Pt−Ir Alloy in the 0.1 M LiOH (H_2O) and 0.1 M LiOH (D_2O) Solutions[a]

		ΔG_θ°	K	r
solution	adsorbate	kJ·mol^{-1}	mol^{-1}	kJ·mol^{-1}
0.1 M LiOH (H_2O)	H	$18.7 < \Delta G_\theta^\circ < 22.2$	$5.3\cdot10^{-4} > K^b > 1.3\cdot10^{-4}$	6.0
0.1 M LiOH (D_2O)	D	$22.2 < \Delta G_\theta^\circ < 25.6$	$1.3\cdot10^{-4} > K^c > 3.3\cdot10^{-5}$	5.7

[a] The Temkin adsorption isotherms are valid and effective only for $0.2 < \theta < 0.8$. [b] $K = 8.6\cdot10^{-4} \exp(-2.4\theta)$ mol^{-1}. [c] $K = 2.1\cdot10^{-4} \exp(-2.3\theta)$ mol^{-1}.

attractive and repulsive interactions is a unique feature of the adsorbed H and D species on the Pt, Ir, and Pt−Ir alloys in acidic and alkaline H_2O and D_2O solutions.

Standard Gibbs Energy of Adsorption. The standard Gibbs energies of adsorption of H and D are given by the differences between the standard molar Gibbs energies of H and D and those of a number of H_2O and D_2O molecules on the adsorption sites of the Pt−Ir alloy surface in the 0.1 M LiOH (H_2O) and 0.1 M LiOH (D_2O) solutions. Under the Frumkin adsorption conditions, the relationship between the equilibrium constants (K) for H and D and the standard Gibbs energies of adsorption (ΔG_θ°) of H and D is[36]

$$2.3RT \log K = -\Delta G_\theta^\circ \quad (8)$$

For the Pt−Ir alloy in 0.1 M LiOH (H_2O) solution, use of eqs 6 and 8 shows that ΔG_θ° of H is in the range $23.2 \geq (\Delta G_\theta^\circ/\mathrm{kJ\cdot mol^{-1}}) \geq 17.7$ for $K = 8.6\cdot10^{-5} \exp(2.2\theta)\ \mathrm{mol^{-1}}$ and $0 \leq \theta \leq 1$. As stated above, this result implies an increase of $|\Delta G_\theta^\circ|$ of H with θ ($0 \leq \theta \leq 1$). It should be noted that ΔG_θ° is a negative number. The standard Gibbs energies (ΔG_θ°) of H and D and the equilibrium constants (K) for the Frumkin and Temkin adsorption isotherms on the Pt−Ir alloy in 0.1 M LiOH (H_2O) and 0.1 M LiOH (D_2O) solutions are summarized in Tables 3 and 4, respectively.

Conclusions

On the Pt−Ir alloy in the 0.1 M LiOH (H_2O) and 0.1 M LiOH (D_2O) solutions, the Frumkin and Temkin adsorption isotherms (θ vs E) of H and D, the equilibrium constants [$K = 8.6\cdot10^{-5} \exp(2.2\theta)\ \mathrm{mol^{-1}}$ for the Frumkin adsorption isotherm and $K = 8.6\cdot10^{-4} \exp(-2.4\theta)\ \mathrm{mol^{-1}}$ for the Temkin adsorption isotherm of H; $K = 2.1\cdot10^{-5} \exp(2.3\theta)\ \mathrm{mol^{-1}}$ for the Frumkin isotherm and $K = 2.1\cdot10^{-4} \exp(-2.3\theta)\ \mathrm{mol^{-1}}$ for the Temkin isotherm of D], the interaction parameters ($g = -2.2$ for the Frumkin isotherm and $g = 2.4$ for the Temkin isotherm of H; $g = -2.3$ for the Frumkin isotherm and $g = 2.3$ for the Temkin isotherm of D), the rates of change of the standard Gibbs energies of adsorption with θ ($r = -5.5\ \mathrm{kJ\cdot mol^{-1}}$ using $g = -2.2$ and $r = 6.0\ \mathrm{kJ\cdot mol^{-1}}$ using $g = 2.4$ for H; $r = -5.7\ \mathrm{kJ\cdot mol^{-1}}$ using $g = -2.3$ and $r = 5.7\ \mathrm{kJ\cdot mol^{-1}}$ using $g = 2.3$ for D), and the standard Gibbs energies of adsorption [$23.2 \geq (\Delta G_\theta^\circ/\mathrm{kJ\cdot mol^{-1}}) \geq 17.7$ for $K = 8.6\cdot10^{-5} \exp(2.2\theta)\ \mathrm{mol^{-1}}$ and $0 \leq \theta \leq 1$ and $18.7 < (\Delta G_\theta^\circ/\mathrm{kJ\cdot mol^{-1}}) < 22.2$ for $K = 8.6\cdot10^{-4} \exp(-2.4\theta)\ \mathrm{mol^{-1}}$ and $0.2 < \theta < 0.8$ in the case of H; $26.7 \geq (\Delta G_\theta^\circ/\mathrm{kJ\cdot mol^{-1}}) \geq 21.0$ for $K = 2.1\cdot10^{-5} \exp(2.3\theta)\ \mathrm{mol^{-1}}$ and $0 \leq \theta \leq 1$ and $22.2 < (\Delta G_\theta^\circ/\mathrm{kJ\cdot mol^{-1}}) < 25.6$ for $K = 2.1\cdot10^{-4} \exp(-2.3\theta)\ \mathrm{mol^{-1}}$ and $0.2 < \theta < 0.8$ in the case of D] have been determined using the phase-shift method and correlation constants.

The value of K decreases in going from H_2O to D_2O. The values of K for both H and D increase with increasing E and θ. For $1 \geq \theta \geq 0$, the value of K for H is approximately 3.7 to 4.1 times greater than that for D. The Frumkin adsorption isotherm is more accurate, useful, and effective than the Temkin adsorption isotherm. For $0.2 < \theta < 0.8$, a lateral attractive ($g < 0$) or repulsive ($g > 0$) interaction between the adsorbed H or D species appears. The duality of the lateral attractive and repulsive interactions is a unique feature of the adsorbed H and D species on the Pt, Ir, and Pt−Ir alloys in acidic and alkaline H_2O and D_2O solutions.

The phase-shift method and correlation constants are the most accurate, useful, and effective ways to determine the Frumkin, Langmuir, and Temkin adsorption isotherms and related electrode kinetic and thermodynamic parameters of noble and highly corrosion-resistant metals (alloys) in acidic and alkaline H_2O and D_2O solutions.

Supporting Information Available:

Other measured values of the phase shift ($-\varphi$) for the optimum intermediate frequency ($f_o = 1.259$ Hz), the estimated fractional surface coverage (θ), and normalized change rates [$\Delta(-\varphi)/\Delta E$ and $\Delta\theta/\Delta E$] of H and D on the Pt−Ir alloy in 0.1 M LiOH (H_2O) and 0.1 M LiOH (D_2O) solutions under the same conditions (Supplementary Tables 1 and 2 and Supplementary Figures 1 and 2, respectively); comparisons of the measured and calculated values of the phase shift ($-\varphi$) for the optimum intermediate frequency ($f_o = 1.259$ Hz) on the Pt−Ir alloy in the 0.1 M LiOH (H_2O) and 0.1 M LiOH (D_2O) solutions (Supplementary Tables 3 and 4, respectively). This material is available free of charge via the Internet at http://pubs.acs.org.

Literature Cited

(1) Gileadi, E.; Kirowa-Eisner, E.; Penciner, J. *Interfacial Electrochemistry*; Addison-Wesley: Reading, MA, 1975.
(2) Gileadi, E. *Electrode Kinetics*; VCH: New York, 1993.
(3) *Electrochemistry and Materials Science of Cathodic Hydrogen Absorption and Adsorption*; Conway, B. E., Jerkiewicz, G., Eds.; Electrochemical Society Proceedings, Vol. 94-21; The Electrochemical Society: Pennington, NJ, 1994.
(4) *Electrochemical Surface Science and Hydrogen Adsorption and Absorption*; Jerkiewicz, G., Marcus, P., Eds.; Electrochemical Society Proceedings, Vol. 97-16; The Electrochemical Society: Pennington, NJ, 1997.
(5) Jerkiewicz, G. Hydrogen sorption at/in electrodes. *Prog. Surf. Sci.* **1998**, *57*, 137–186.
(6) *Hydrogen at Surfaces and Interfaces*; Jerkiewicz, G., Feliu, J. M., Popov, B. N., Eds.; Electrochemical Society Proceedings, Vol. 2000-16; The Electrochemical Society: Pennington, NJ, 2000.
(7) Gileadi, E. In *Electrosorption: Adsorption in Electrochemistry*; Gileadi, E., Ed.; Plenum Press: New York, 1967; pp 1−18.
(8) Chun, J. H.; Ra, K. H. The phase-shift method for the Frumkin adsorption isotherms at the Pd/H_2SO_4 and KOH solution interfaces. *J. Electrochem. Soc.* **1998**, *145*, 3794–3798.
(9) Chun, J. H.; Ra, K. H.; Kim, N. Y. The Langmuir adsorption isotherms of electroadsorbed hydrogens for the cathodic hydrogen evolution reactions at the Pt(100)/H_2SO_4 and LiOH aqueous electrolyte interfaces. *Int. J. Hydrogen Energy* **2001**, *26*, 941–948.
(10) Chun, J. H.; Ra, K. H.; Kim, N. Y. Qualitative analysis of the Frumkin adsorption isotherm of the over-potentially deposited hydrogen at the poly-Ni/KOH aqueous electrolyte interface using the phase-shift method. *J. Electrochem. Soc.* **2002**, *149*, E325−330.
(11) Chun, J. H.; Ra, K. H.; Kim, N. Y. Langmuir adsorption isotherms of over-potentially deposited hydrogen at poly-Au and Rh/H_2SO_4 aqueous electrolyte interfaces: Qualitative analysis using the phase-shift method. *J. Electrochem. Soc.* **2003**, *150*, E207−217.
(12) Chun, J. H. Methods for estimating adsorption isotherms in electrochemical systems. U.S. Patent 6,613,218, 2003.
(13) Chun, J. H.; Jeon, S. K.; Kim, B. K.; Chun, J. Y. Determination of the Langmuir adsorption isotherms of under- and over-potentially deposited hydrogen for the cathodic H_2 evolution reaction at poly-Ir/aqueous electrolyte interfaces using the phase-shift method. *Int. J. Hydrogen Energy* **2005**, *30*, 247–259.
(14) Chun, J. H.; Jeon, S. K.; Ra, K. H.; Chun, J. Y. The phase-shift method for determining Langmuir adsorption isotherms of over-potentially deposited hydrogen for the cathodic H_2 evolution reaction at poly-Re/aqueous electrolyte interfaces. *Int. J. Hydrogen Energy* **2005**, *30*, 485–499.
(15) Chun, J. H.; Jeon, S. K.; Kim, N. Y.; Chun, J. Y. The phase-shift method for determining Langmuir and Temkin adsorption isotherms of over-potentially deposited hydrogen for the cathodic H_2 evolution reaction at the poly-Pt/H_2SO_4 aqueous electrolyte interface. *Int. J. Hydrogen Energy* **2005**, *30*, 1423–1436.
(16) Chun, J. H.; Kim, N. Y. The phase-shift method for determining adsorption isotherms of hydrogen in electrochemical systems. *Int. J. Hydrogen Energy* **2006**, *31*, 277–283.
(17) Chun, J. H.; Jeon, S. K.; Chun, J. Y. The phase-shift method and correlation constants for determining adsorption isotherms of hydrogen at a palladium electrode interface. *Int. J. Hydrogen Energy* **2007**, *32*, 1982–1990.
(18) Chun, J. H.; Kim, N. Y.; Chun, J. Y. Determination of adsorption isotherms of hydrogen and hydroxide at Pt−Ir alloy electrode interfaces

using the phase-shift method and correlation constants. *Int. J. Hydrogen Energy* **2008**, *33*, 762–774.
(19) Chun, J. Y.; Chun, J. H. Correction and supplement to the determination of the optimum intermediate frequency for the phase-shift method [Chun et al., Int. J. Hydrogen Energy 30 (2005) 247−259, 1423−1436]. *Int. J. Hydrogen Energy* **2008**, *33*, 4962–4965.
(20) Chun, J. Y.; Chun, J. H. A negative value of the interaction parameter for over-potentially deposited hydrogen at Pt, Ir, and Pt−Ir alloy electrode interfaces. *Electrochem. Commun.* **2009**, *11*, 744–747.
(21) Chun, J. Y.; Chun, J. H. Determination of adsorption isotherms of hydrogen on titanium in sulfuric acid solution using the phase-shift method and correlation constants. *J. Chem. Eng. Data* **2009**, *54*, 1236–1243.
(22) Chun, J. H.; Chun, J. Y. Determination of adsorption isotherms of hydrogen on zirconium in sulfuric acid solution using the phase-shift method and correlation constants. *J. Korean Electrochem. Soc.* **2009**, *12*, 26–33.
(23) Chun, J.; Lee, J.; Chun, J. H. Determination of adsorption isotherms of overpotentially deposited hydrogen on platinum and iridium in KOH aqueous solution using the phase-shift method and correlation constants. *J. Chem. Eng. Data* **2010**, *55*, 2363–2372.
(24) Chun, J.; Kim, N. Y.; Chun, J. H. Determination of adsorption isotherms of hydroxide and deuteroxide on Pt−Ir alloy in LiOH solutions using the phase-shift method and correlation constants. *J. Chem. Eng. Data* **2010**, *55*, 3825–3833.
(25) Kvastek, K.; Horvat-Radošević, V. Comment on: "Langmuir adsorption isotherms of over-potentially deposited hydrogen at poly-Au and Rh/H_2SO_4 aqueous electrolyte interfaces. Qualitative analysis using the phase-shift method" [J. Electrochem. Soc., 150, E207 (2003)]. *J. Electrochem. Soc.* **2004**, *151*, L9–L10.
(26) Lasia, A. Comments on "The phase-shift method for determining Langmuir adsorption isotherms of over-potentially deposited hydrogen for the cathodic H_2 evolution reaction at poly-Re/aqueous electrolyte interfaces" [Hydrogen Energy 30 (2005) 485−499]. *Int. J. Hydrogen Energy* **2005**, *30*, 913–917.
(27) Horvat-Radošević, V.; Kvastek, K. Pitfalls of the phase-shift method for determining adsorption isotherms. *Electrochem. Commun.* **2009**, *11*, 1460–1463.
(28) Chun, J. H.; Ra, K. H.; Kim, N. Y. Response to "Comment on: 'Langmuir adsorption isotherms of over-potentially deposited hydrogen at poly-Au and Rh/H_2SO_4 aqueous electrolyte interfaces: Qualitative analysis using the phase-shift method'" [Journal of the Electrochemical Society, 150, E207 (2003)]. *J. Electrochem. Soc.* **2004**, *151*, L11–L13.
(29) Chun, J. H.; Jeon, S. K.; Kim, N. Y.; Chun, J. Y. Response to comments on: The phase-shift method for determining Langmuir adsorption isotherms of over-potentially deposited hydrogen for the cathodic H_2 evolution reaction at poly-Re/aqueous electrolyte interfaces: [Hydrogen Energy 30 (2005) 485−499]. *Int. J. Hydrogen Energy* **2005**, *30*, 919–928.
(30) In our e-mail communications, Horvat-Radošević and Kvastek admitted that all of their objections to the phase-shift method in ref 27 were confused and misunderstood. The exact same confusion and misunderstanding about the phase-shift method also appear in refs 25 and 26. They still do not understand and accept the phase-shift method itself without reliable simulation or experimental data.
(31) Gileadi, E.; Kirowa-Eisner, E.; Penciner, J. *Interfacial Electrochemistry*; Addison-Wesley: Reading, MA, 1975; pp 6 and 72−73.
(32) Gileadi, E.; Kirowa-Eisner, E.; Penciner, J. *Interfacial Electrochemistry*; Addison-Wesley: Reading, MA, 1975; pp 86−93.
(33) Gileadi, E. *Electrode Kinetics*; VCH: New York, 1993; pp 291−303.
(34) Harrington, D. A.; Conway, B. E. AC impedance of faradaic reactions involving electrosorbed intermediates-I. Kinetic theory. *Electrochim. Acta* **1987**, *32*, 1703–1712.
(35) Gileadi, E.; Kirowa-Eisner, E.; Penciner, J. *Interfacial Electrochemistry*; Addison-Wesley: Reading, MA, 1975; pp 82−86.
(36) Gileadi, E. *Electrode Kinetics*; VCH: New York, 1993; pp 261−280.
(37) Bockris, J. O'M.; Reddy, A. K. N.; Gamboa-Aldeco, M. *Modern Electrochemistry*, 2nd ed.; Kluwer Academic/Plenum Press: New York, 2000; Vol. 2A, pp 1193−1197.
(38) Oxtoby, D. W.; Gillis, H. P.; Nachtrieb, N. H. *Principles of Modern Chemistry*, 5th ed.; Thomson Learning Inc.: New York, 2002; p 446.
(39) Gileadi, E. *Electrode Kinetics*; VCH: New York, 1993; pp 303−305.

Received for review April 25, 2010. Accepted November 6, 2010. This work was supported by a Sabbatical Year Grant from Kwangwoon University in 2009.

JE100418N